Journal Pre-proof

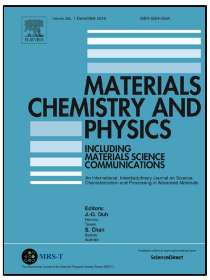

Novel Fractal Analysis of Nanograin Growth in BaTiO3 Thin Film

Habibollah Aminirastabi, Hao Xue, Vojislav V. Mitić, Goran Lazović, Gouli Ji, Dongliang Peng

PII:	S0254-0584(19)31076-4
DOI:	https://doi.org/10.1016/j.matchemphys.2019.122261
Reference:	MAC 122261
To appear in:	*Materials Chemistry and Physics*
Received Date:	15 May 2019
Accepted Date:	04 October 2019

Please cite this article as: Habibollah Aminirastabi, Hao Xue, Vojislav V. Mitić, Goran Lazović, Gouli Ji, Dongliang Peng, Novel Fractal Analysis of Nanograin Growth in BaTiO3 Thin Film, *Materials Chemistry and Physics* (2019), https://doi.org/10.1016/j.matchemphys.2019.122261

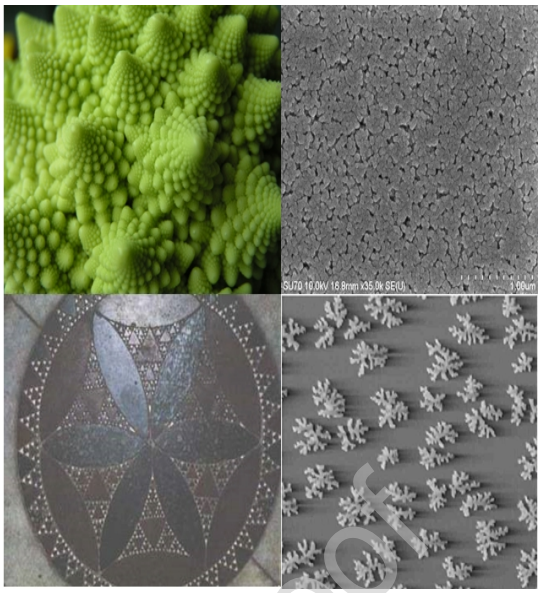

Novel Fractal Analysis of Nanograin Growth in BaTiO3 Thin Film

Habibollah Aminirastabi[1], Hao Xue [2], Vojislav V. Mitić[3], Goran Lazović[4], Gouli Ji[5], Dongliang Peng[6]

College of Materials, Xiamen University, Xiamen, Fujian province, China, 361005[1, 6, 2];
Faculty of Electronic Engineering – University of Nis, Nis, 18000, Serbia[3];
Institute of Technical Sciences – SASA, Belgrade, 11000, Serbia[3];
Faculty of Mechanical Engineering – University of Belgrade, 11000, Serbia[4];
School of Aerospace Engineering, Xiamen university, Xiamen, Fujian province, China, 361005[5].

Abstract

The grain size and the ferroelectric morphology are the two most important factors in the research and development of advanced dielectric devices. It is important to synthesize nanostructures in order to achieve optimal grain size and inhibit grain growth while controlling the sintering parameters. It is also important to find new methods to study the grain growth during densification. BaTiO3 films were successfully obtained via the sol-gel spin coating method.
In this paper, we report the deposition of nanostructured BaTiO3 thin film by spin coating of sol-gel precursors. The densification, grain growth and microstructure evolution have been studied. Moreover, a novel physical and mathematical fractal analysis have been applied successfully to the densification and nano grain growth of BaTiO3 thin film. The discrepancy between the fractal dimension and the grain growth with increasing temperatures and soaking time are presented and discussed.

Keywords: $BaTiO_3$, grain growth, fractal dimension, self-similarity, sol-gel route

1. Introduction

$BaTiO_3$, with perovskite structure, has many applications. It has dielectric with values as high as 7,000, much greater than those of other ceramics, such as TiO_2 (ε_r=110). The solid $BaTiO_3$ can exist in five phases: a hexagonal crystal structure, which ranges from high to low temperatures; a cubic structure; a tetragonal orthorhombic structure; and a trigonal structure. All of these phases, except the cubic phase, exhibit ferroelectric properties [1, 2].

$BaTiO_3$, with piezoelectric properties, is used in microphones, transducers, small-sized multi-film capacitors in high-voltage capacitors, memory applications, sensors, actuators, and electro-optic industries. $BaTiO_3$ is a lead-free ferroelectric material and a good alternative to lead zirconate titanate. It is used in various forms: crystalline, bulk ceramic, multilayer, and thin films [3-6]. In addition to having applications in the miniaturization of many modern systems such as microwave components, it can also be integrated into microelectronic circuits to achieve desirable physical properties, in which case, small grains on a submicron or nanometer scale are used [7,8]. The biggest obstacle to developing the high-capacity multilayered ceramic capacitors is achieving

the optimal grain size of $BaTiO_3$-ceramics. The reduction of dielectric layer thickness demands the simultaneous reduction of $BaTiO_3$ grain size to a submicron level [9].

The electrical properties of $BaTiO_3$ are dependent on grain size, density, pore size and pore size distribution, morphology, impurity, and defect concentration; all these factors directly affect the grain growth kinetics. Usually for ceramic grain size more than 1 μm when the grain size decreases, the dielectric constant at room temperature increases. However, the temperature dependence of the dielectric constant was modified significantly below the Curie temperature (TC), when grain size reduces below 1 μm. The dielectric constant of BaTiO3 shows a maximum of ~5000 for grains in the range of 0.8–1 μm which was attributed to critical changes in the domain structure. On further decrease of grain size, dielectric constant rapidly decreases below 1000 [52,53]. For the commercially available Multilayer energy storage ceramic capacitors use dielectric layers with thicknesses 1 μm or less. Accordingly, the grain size of these ferroelectric ceramics should be approximately 50-150 nm to meet the temperature stability requirement and to maintain reliable performance [54]. Density increases with the sintering time and temperature during the grain growth [11, 12]. Retaining nanoscale grain size and preventing rapid grain growth are the main challenges encountered in the nanoparticle sintering process [10].

We know that the grains grow during the sintering process. We cannot stop the growing process completely. We can only reduce their growth rate and examine the parameters effectively. We are looking for one fundamental question: Is there a tool that can analyze the changes in grains during the process collectively?. So that, at first, it introduces fractal and then produce same grain in small scales with sol-gel? The fractal analysis has significantly influenced our comprehension of complex structures and dynamic procedures in an extensive variety of natural and industrial phenomena [15-16]. A fractal refers to an object comprised of smaller parts that are smaller versions of the whole and every little piece imitates the entire structure. At a higher level of magnification, a similar pattern will keep reemerging to such an extent that it is relatively difficult to know precisely what scale you are looking at [17]. This property is also called “scale-invariance”, the most essential feature of fractals, which is also referred to as “self-similarity”. [18]. This feature enables fractals to be analyzed scientifically, making it more understandable when connected to an assortment of controls. Researchers and specialists have analyzed fractals all over the world [21-26].

They all have one thing in common: they grow. In materials science, fractals are constrained to geometry but can be utilized to depict the properties of periodic arrangement [31-44]. Fractal changing, due to pores and variance in grain boundaries, can be used as an indication of grain growth during the sintering process in ceramics. Fractal dimensions could be used to describe complex phenomena such as grain growth and aggregations of nanograin in molecular systems at the atomic scale. In general, the computation of the fractal dimension by the box-counting method underestimates the true D_f, mainly due to the discretization of the image domain and the quantization of the gray levels [45, 46]. We do base this paper on proving our own scientific hypothesis based on fractal creation but, considering the nature as well as studying the development of cases in different situations, this fact is acceptable. However, why is it that it has not been highlighted is because of the lack of relation between fractal, grain, and pore growth? If we put together growth and fractals, many scientific issues will be easier to explain. In general, the process of depositing thin films is divided into three major methods: the chemical vapor deposition (CVD), the physical vapor deposition, and wet deposition. Sol-gel processing is used in the synthesis of colloidal dispersions of inorganic and organic-inorganic hybrid materials obtained by introducing certain organic permanent groups. Spin coating is used for thin film growth from sol-gel solution on a flat substrate. The sol-gel process has many advantages,

including higher purity and homogeneity and lower processing temperature. It also allows for the control of nucleation and growth of primary colloidal particles, as well as the control of the entire process and the synthesis of "tailor-made" materials, which can be used to obtain the distribution of special shapes and sizes [13, 14].

In this research, we prepared BaTiO3 films using the sol-gel method and investigated the influence of sintering conditions, temperature, and soaking time on the grain parameters that affect the microstructure of the sample. Fractal dimensions, as a characterization microstructure, describe the relations between grain growth kinetics and grain microstructure, and trace any changes in grain microstructure that occur during the sintering process. This method can be used by a machine to control, engineer, and monitor microstructures under different conditions.
It uses a large number of images such as the SEM images to increase the accuracy of a machine.
As such, it saves a lot of costs and prevents any unnecessary work on the part of a researcher. Furthermore, we can set time for a machine using fractal analysis and make artificially intelligent machines to synthesize materials in the future.

2. Experiment

2.1. Experimental material

In this research, $BaTiO_3$ thin films with nanocrystal grains were synthesized using a sol-gel route [Fig. 1]. Barium acetate (Ba $(CH_3COO)_2$) and tetrabutyl titanate ($Ti(OC_4H_9)_4$) were used as the main substrate reagents and acetic acid (CH_3COOH) and ethyl alcohol were the solvents. Barium acetate, dissolved in acetic acid, was mixed with polyvinylpyrrolidone, dissolved in ethyl alcohol and acetyl acetate, and then added to tetrabutyl titanate. Then, it was stirred for an hour to form $BaTiO_3$ precursor at room temperature.

High-resistance (coated with ITO (indium tin oxide)) silicon wafers were used as substrates for depositing $BaTiO_3$ coatings.

Before depositing the layers, the silicon wafers were washed and cleaned with ethyl alcohol, acetone, and ammonium to eliminate adsorbed impurities and to form a stable film.

The substrates are dried and placed in a centrifuge along with the sol-gel solution. The centrifuge is set at 3000 revolutions per minute (RPM) for 60 seconds, coating the substrates with an even distribution of the sol-gel solution. One batch was then sintered at different temperature (300-800°C) and the same soaking time (2 hours).
Other samples were held at the same temperature (700°C) for a different soaking time (1 to 600 minutes), and then left in the furnace to cool down. To study the grain growth during the sintering process, the specimens were heated in a typical furnace filled with atmospheric air and the temperature was increased by 3°C/min.
The crystallization process of $BaTiO_3$ gel was studied with the aid of DSC/TG (German NETZSCH, STA449 F3), and XRD (powder diffractometer). The microstructure of the films was examined using SEM (Hitachi SU-70) and TEM JEM-2100. The grain size of $BaTiO_3$ nanocrystals was determined using image analysis with software IMAGE J. We will explain this procedure in more detail in the paper. Fractal dimensions were calculated using FRACTAL ANALYSIS SYSTEM version 3.4.7. It has the ability to make image files in different formats and calculate fractal dimensions from color image, grayscale, binary, 3D-sliced (layer) so in this paper fractal dimension has been calculated by the method of box-counting after being changed to grayscale $2<D_F<3$).

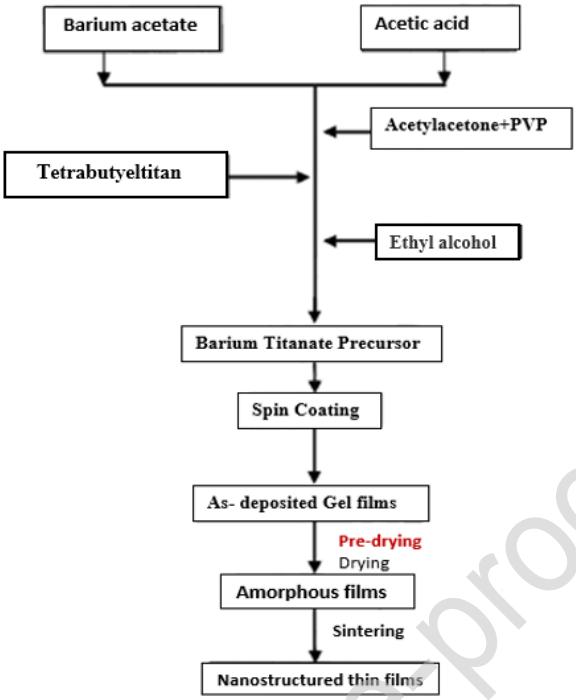

Fig. 1. The process for the preparation of $BaTiO_3$ film by sol-gel route.

2.2. Experimental fractal analysis

Fractal dimension that we have obtained in our paper is obtained using the box-counting method. In the additional Hausdorff dimension, box counting is a method that is suitable for obtaining the relationship between objects. The box-counting method is used to analyze patterns by breaking and classifying them into object, dataset, image, etc, small pieces that machine can calculate and recognize. The nature of the process is compared by zooming in or out of optical and computational methods to analyze and check how detailed observations vary with scale [Fig. 2]. To measure closeness of a pre-fractal B, that approximates an ideal fractal A, the Hausdorff distance, given by:

$$d_h(A, B) = \max\{\max\{d(y, A), y \in B\}, \max\{d(x, B), x \in A\}\} \quad (1)$$

where d(s, A) is the distance of a point s to the set A (see [40]).

Keeping in mind the notion of the Hausdorff distance DH, it is not difficult to understand that self-similarity, which is equivalent to scale invariance, is a direct consequence of contractive (or dilation) symmetry [48]. Namely, the usual meaning of being symmetric understands that, for a symmetric object S, there exists transformation T so that, if T has a unit norm, T does not change the size of the object. It just transforms the object inside itself. On the other hand, for the fractal object S, there is the transformation T that satisfies $||T||<1$ so that: $T(S)=S$.
In this case, T is called the transformation of dilation symmetry. To prove the testing procedure and approve the methodology, some explanations have been presented to make the scientific

nature of the procedure clear. The topological DT (general dimensions, visual dimensions, and Euclidean dimensions, DT = 1 for curves, 2 for surfaces, 3 for solids, etc.) is much smaller than the Hausdorff DH (normal DT expansion), DT <DH. Contrary to the topological dimension, the Hausdorff size (or fractal) DH is typically a non-integral number for a fractal object, while DH = DT is for Euclidean objects. Example: Liquid level DT = DH = 2, that is, the surface layer of liquid molecules (approximately) is a mathematical one. Any disorder caused by the former, through heating the geometry of the surface will be complicated, with 2 <DH<3. Upper limit DH = 3 with the evaporation of all liquid particles, the flat layer transforms into a part of the 3D space [40].

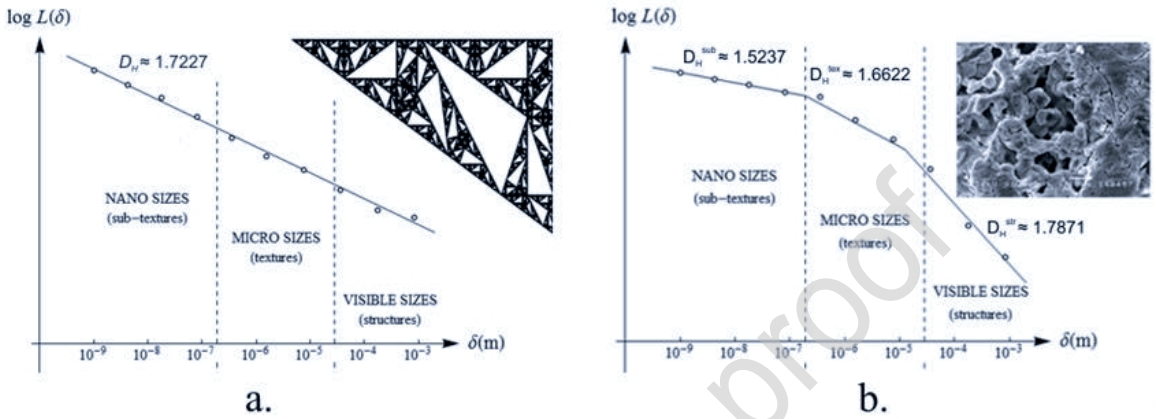

Fig. 2. The Richardson-Mandelbrot diagram for: a. Mathematical fractal (Conway triangle, DH ≈ 1.7227); b. Real fractal – the SE microphotograph of BaTiO3 ceramics doped with 0.1 wt% of Holmium (Ho2O3). Fractal dimensions differ in various ranges of magnitude, as expected from real fractals (pre-fractals) [49].

Fractal objects can be classified by their fractal dimension. Fractal dots (usually called fractal dust) with DT = 0 and 0 < DH < 1 (ex. Cantor set), fractal lines, DT = 1 and 1 < DH < 2 (ex. Koch snowflake, [10]), fractal surface DT = 2 and 2 < DH < 3 (ex. Menger sponge), etc. [42].

3. Results and discussion

3.1. The characterization of BaTiO3 nanocrystals

The thermal decomposition of BaTiO3 sol-gel solution after heating (40°C, 24 hours) in air was studied by using DTA/TG. [Fig. 3] shows the results. As can be seen, the total weight loss of the sol-gel reaches 60.92% from 30°C to 800°C. Normally, the decomposition of a composite containing polymer can be divided into four steps. The first step is in the temperature range of 30-110°C. The weight-loss at this stage is about 4.88%, which can be attributed to the emission of water vapor. The second stage is in the temperature range of 110-250°C and the corresponding weight loss is about 7.59%, which can be attributed to the emission of organic solvents. The third step is in the temperature range of 250-450°C. The corresponding weight loss is 37.53%, which can be attributed to the combustion of organic materials within the framework of the gel. On the DTA curve, no significant thermal effect was observed in the second or the third steps. The last step is in the temperature range of 450-800°C. The corresponding weight loss is 10.92%. On the DTA curve, endothermic and exothermic peaks at 470°C and 560°C, A, B points, respectively, appear due to polymer decomposition and the initial formation of $BaTiO_3$. The weight loss in this stage is probably due to the combustion of carbon materials, the last element of polyvinylpyrrolidone.

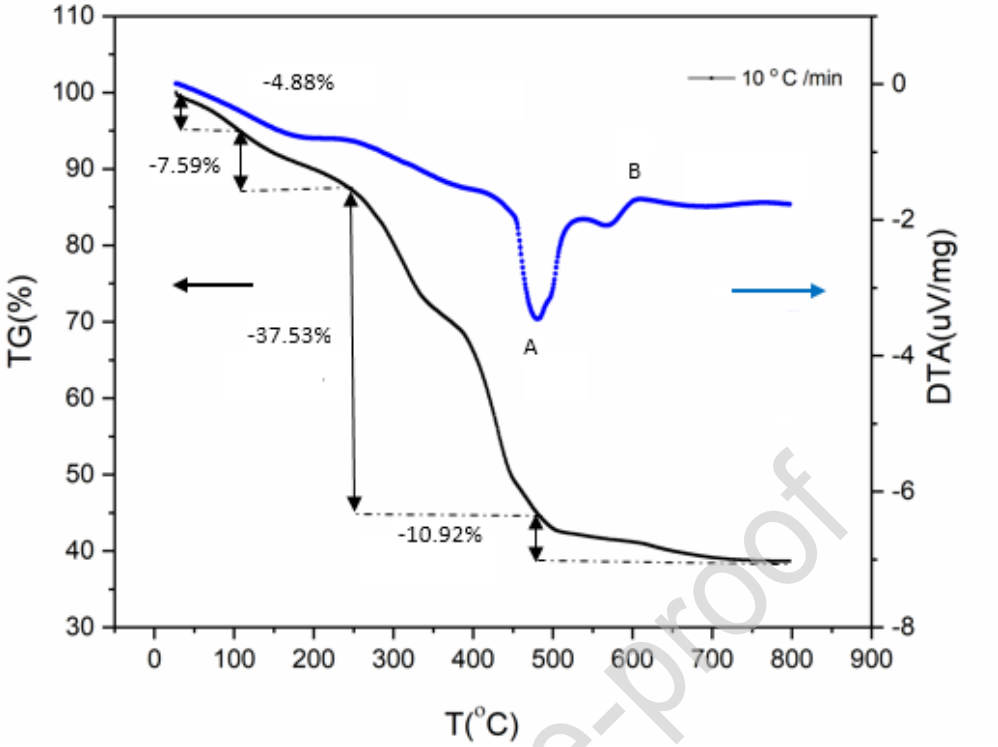

Fig. 3. DTA/TG curves of the $BaTiO_3$ nanocrystal precursor of the sample.

The XRD patterns of the $BaTiO_3$ film obtained after being sintered under different conditions are shown in [Fig. 4(a)] and [Fig. 4(b)].

After increasing calcination temperature from 300°C to 800°C (duration=2 h), the main diffraction peaks of BaTiO3 heated to 700°C for 2 hours become narrower and sharper than those at other temperatures. [Fig. 4(a)] indicates that a calcination temperature (300-500°C with a 2-hour soaking time) is not enough high for the BaTiO3 grain to be completely sintered and the probability of forming initial seeds at this temperature is higher than at other temperatures.

By increasing the temperature of the coating materials from 300 to 800°C, the diffraction peak for the (1 1 1) planes of thenanograined BaTiO3(BTO) ceramics heated to around 600°C shifts 2 theta of from 38.8 to 38.98. This indicates that the tetragonality of the samples was increased [Fig. 4(a)]. Other diffraction peaks of the nanograined BTO ceramics shift in a similar way as the (1 1 1) peak does, with variation in the sintering temperature as well as the amount of the coating materials.

After increasing the soaking time from 3 min to 600 min (T = 700°C), as indicated by [Fig. 4(b)], upon calcination at 700°C for more than 100 mins, the peak intensity is sharper and narrower than that of the times less than 100 min. This implies that thermal aging (> 100 min) at a temperature as high as 700°C is necessary for the complete crystallization of $BaTiO_3$ and the complete removal of carbon from the product. For comparison, the peak ratio of XRD patterns between $BaTiO_3$ and ITO (indium tin oxide) is used.

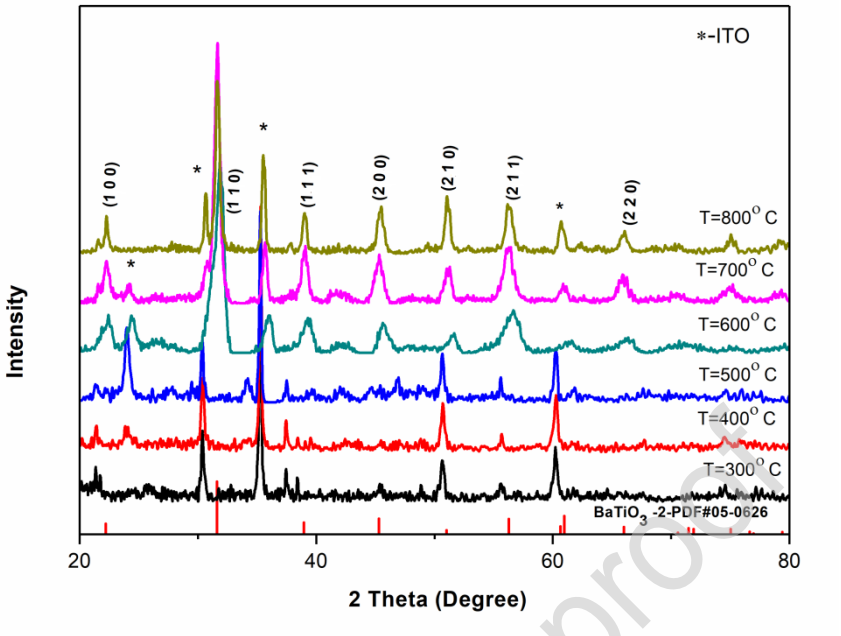

FiG. 4 (a). The XRD patterns of $BaTiO_3$ films at 300°C to 800° C for 2 hours.

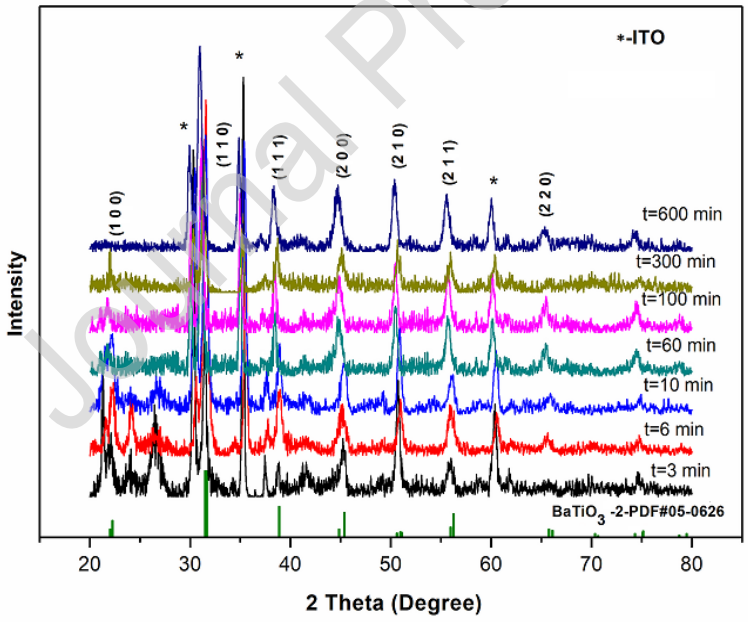

Fig. 4 (b). The XRD patterns of $BaTiO_3$ films at 700°C from 3 min to 600 min.

The transmission spectrum of the thin films at different temperatures using the same soaking time is shown in [Fig. 4 (c)]. For comparison, the transmission curve of a bare ITO-coated glass is also included. It can be seen that the films deposited on the ITO-coated glass and ITO is different in the spectral range from 500 cm^{-1} to 1600 cm^{-1}. The high transparency at 700°C indicates small surface roughness and relatively good homogeneity of the film. The transmission decreases

sharply when the structure, that has certain polymers and wavelength, is reduced to around 500 cm^{-1} to 800 cm^{-1} for samples (b-e), showing inter-band transitions.

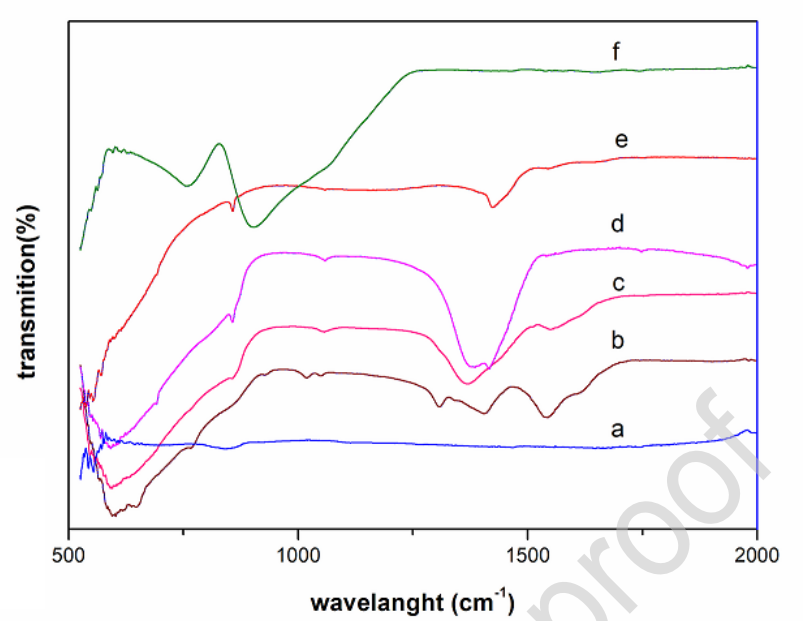

Fig. 4 (c). The transmittance spectra of ITO, ITO/BTO films sintered at various temperatures for 2 hours: (a) ITO, (b) 300° C, (c) 400° C, (d) 500° C, (e) 600° C and (f) 700° C.

The coating processes around the grains like ITO material are very complex and very sensitive for analysis. Our research generated different expiriences and knowledges about effects of coating phenomena. The BaTiO3 thin films penetrate through surrounded microstructure morphology to grain cores and creating microstructures which are different than before coating process. In this research aspects there are a lot open questions. Some of this analysis are explaining that the results of coating processes are not always completelly succesful around the grains and related thin films which should surround the grains. The reliability of succesful coating process around the grains is still under the deeper research. But different scientific analysis in this area definitelly confirm that we are getting changed morphologies. So, different characteristics are changing in a correspondance to this microstructure changes. Results in this research paper on this topic are confirmation regarding the discussion which we gave in previous analysis. Based on concrete results in this research paper it is evident that transmission lines on Fig. 4(c) are confirming the evident differences between the samples with no coating in comparison with samples which past coating process. The temperature growth from 300 to 700℃ just confirm the microstructure changes in the samples under coating process affected by temperature growth. This is on the line with grains growth temperature dependance analysis, what is the topic of main importance in our research.

In future scientific research which results are on the way, it should be the one important key point for further clarifications and explanations.

3.2. The grain growth and kinetics of grain growth $BaTiO_3$ nanocrystals

3.2.1. Grain growth during a heat-up and a 2-hour soaking time

The morphology of the nanosized barium-titanate is shown in [Fig. 5(a)]. The images of layers at 300°C to 700°C are obtained in bulk layers and are not exactly clear because the structure of layers within these temperatures contains a large number of polymers, especially at temperatures less than 500°C. Using the image analysis technique, the average grain size of $BaTiO_3$ film can be calculated. After sintering at 300°C to 800°C with a soaking time of 2 hours, average grain sizes were from 25 nm to 130 nm, approximately. The plots of average grain size during a heat-up and a 2-hour soaking time are displayed in [Fig. 5(b)].

The rapid grain growth during this sintering stage is easily observed in [Fig. 5(a, b)] after sintering at 800°C. So, at 700°C and a 2-hours soaking time, the nanostructure is preserved. Therefore, by increasing the time factor, we can increase our density and make a nano-homogeneous structure. Also, with the microstructure monitoring, abnormal grain growth is prevented.

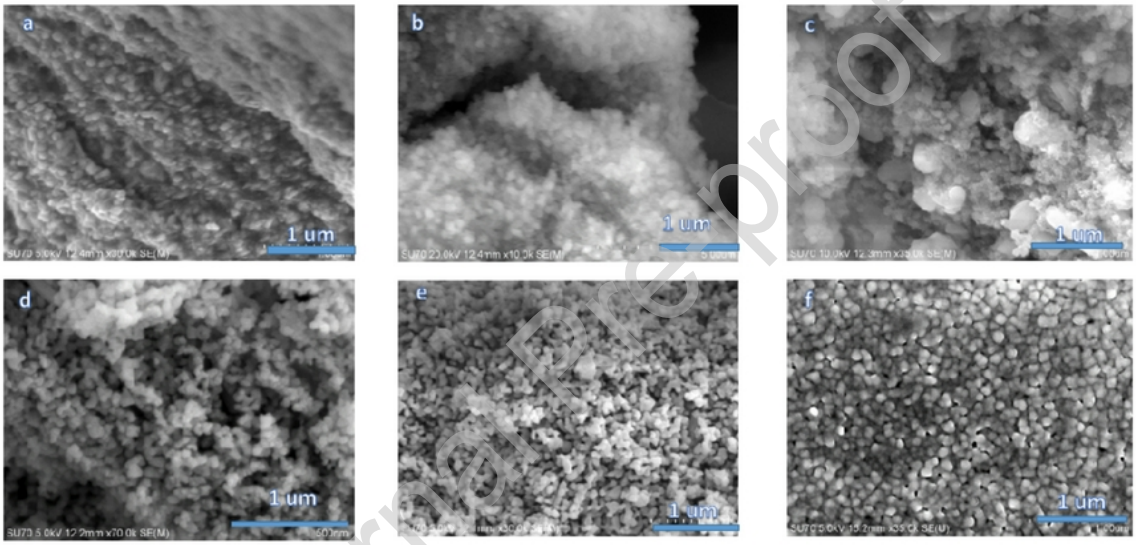

Fig. 5 (a). The SEM Micrographs of $BaTiO_3$ sintered at (a) 300°C; (b)400°C; (c)500°C; (d)600°C; (e)700°C; and (f)800°C for 2 hours.

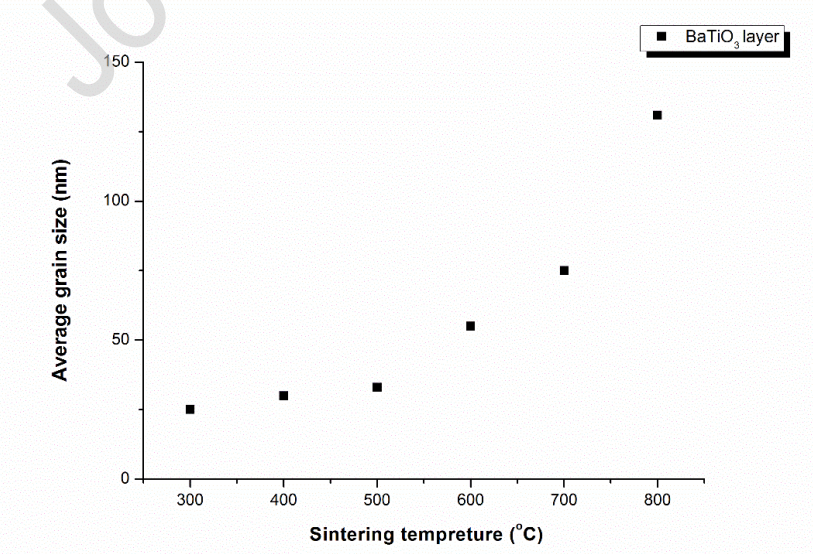

Fig. 5 (b). The BaTiO3 grain growth during heat up at 300°C to 800°C for a 2-hour soaking time.

3.2.2. The relationship between fractal dimensions, grain boundary, and pores

During the grain growth process, the microstructure, including the grain area, grain perimeter, the volume of grain and pores, and the surface of grain boundary, will be changed. They are correlated so they scale up [19, 27].

The range of the fractal dimension is between 2 and 3 ($2<D_F<3$). Generally speaking, a higher dimension is related to a rougher surface with higher porosity.

$$P_G^{1/D_F} \propto A_G^{1/2} \tag{2}$$

Here, P_G is the perimeter of the grain boundary and A_G is the area of grain;

$$A_G^{1/D_F} \propto V_G^{1/3} \tag{3}$$

where A_G is the surface area of the grain boundary and V_G is the grain volume. They can be transformed and simplified into logarithmic forms,

$$\text{Log } P_G = D_F/2 \text{ log } A_G + C_1 \tag{4}$$

and

$$\text{Log } A_G = D_F/3 \text{ log } V_G + C_2 \tag{5}$$

Boming Yu provides the method for judging whether porous material could be analyzed using fractal theory [55, 56]:

$$\left(\lambda_{\min} / \lambda_{\max}\right)^{D_F} = 0 \tag{6}$$

where $\lambda_{\min}$, $\lambda_{\max}$ are the minimal and the maximal values of pore diameter and D_F is the fractal dimension. The pore distribution of the porous structure should meet the scaling invariance within a certain range, $2<D_F<3$.

Guo et al. deduced [56]:

$$\text{Log } S = (3-D_F) \text{ Log } r + C \tag{7}$$

where *S* is the cumulative pore volume fraction; D_F is the fractal dimension; and r is the pore diameter. So, when structural pores are omitted, the main density is near the theoretical density, the surface is flat, and the fractal dimension decreases.

[Fig. 5(c)] shows variation of fractal dimension of nanostructure $BaTiO_3$ at different temperatures with 2 hours soaking time. According to this figure, surface of layer will be smooth after heat treatment at 600°C which will, thus, lead to the decrease of the fractal dimension before the temperature of 600°C, due to the presence of polymer. The surface of the sample looks smooth and without any porosity, so the fractal number is close to 2. It can be observed that the size of the fractal dimension does not depend on a selected area (every box in [Fig. 5(c)] shows pixel of the selection area).

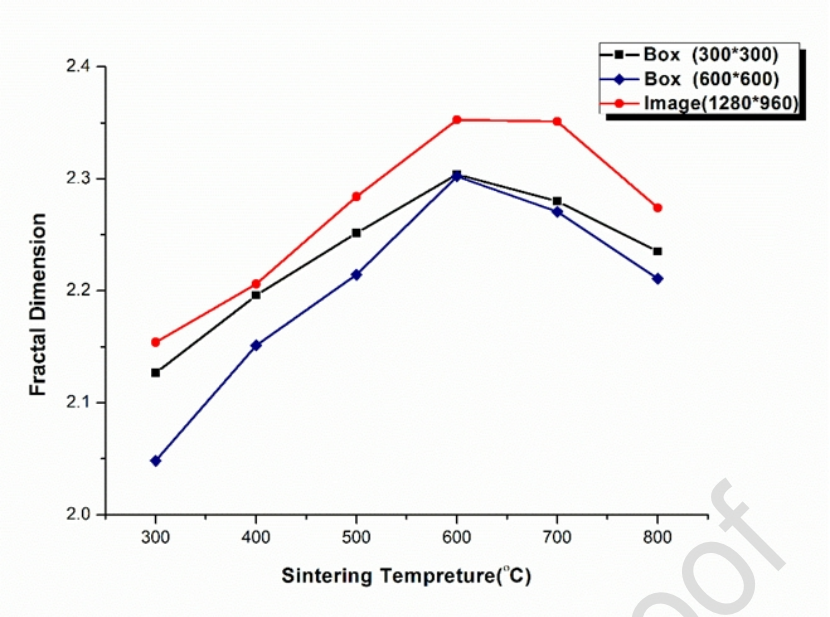

Fig. 5 (c). The variation of the fractal dimension of nanostructure BaTiO3 at different temperatures for 2 hours

The substance of the matter is definitelly introducing the fractal nature analysis and fractal dimensions what is quite new approach in the science of sintering processes. Our previous results with fractal corrections confirmed that there is existance of result changes affected by the fractalization research results. So, the differences-discrepancies with grain growth without fractal analysis and with it, are just confirming our expectations because the fractal scientific view more precisely and with higher level of complexity define many relations between the structure and parameters especially the temperature. So, all of this presented results just confirm the fractal nature existance in ceramics and widely different materials.

3.2.3. Grain growth during isothermal holdings

At 700°C, after gradually removing the carbon impurity, the grains in the $BaTiO_3$ layers with the thicknesses of around 800 nm grow faster. The porosity is removd and the surface is smothered [Fig. 6, 7]. Its mean surface will be flat and, in the bulk of the ceramic, the grain will become larger and larger during the sintering process. In order to understand the entire grain growth process, isothermal sintering experiments were carried out at 700°C following a heat-up at 3°C/min.

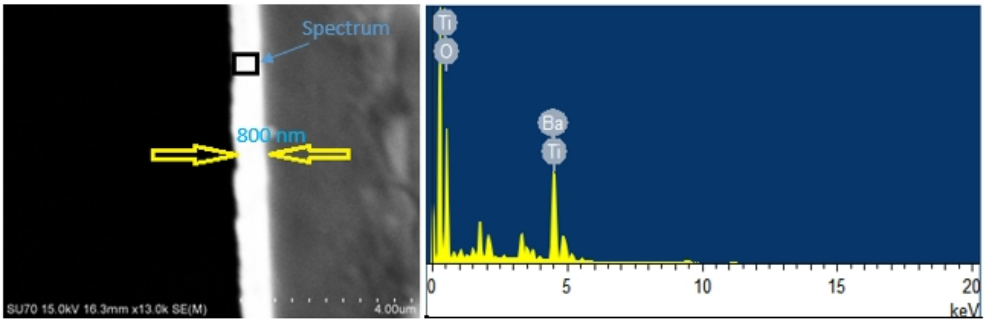

Fig. 6. The SEM Micrographs of $BaTiO_3$ layer sintered at 700°C for 300 minutes.

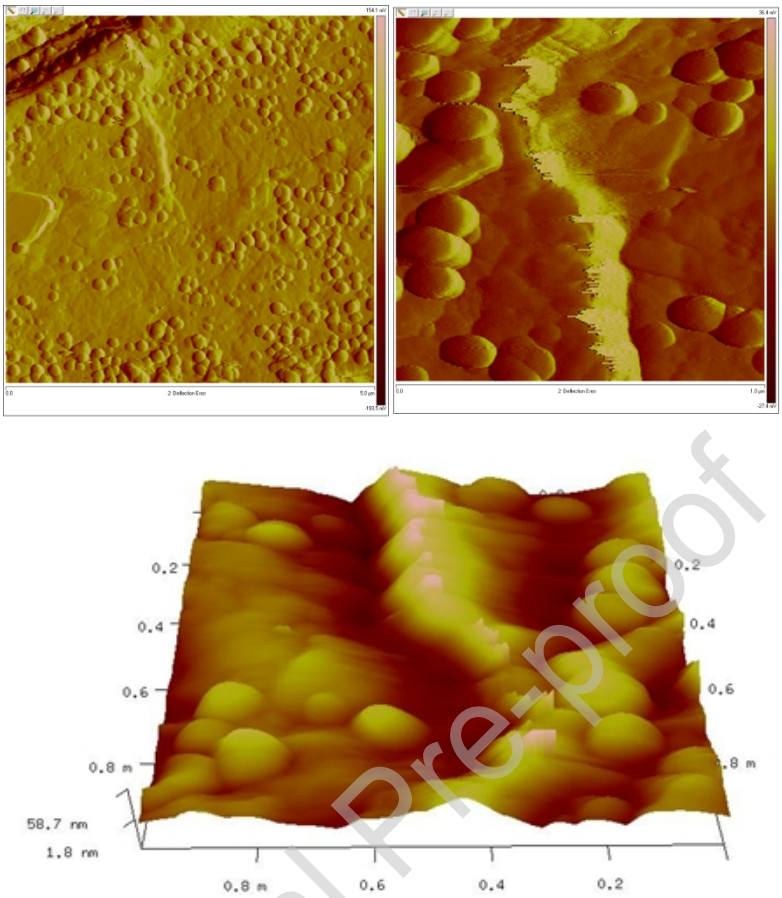

Fig. 7. The AFM micrographs of the BaTiO3 films, deposited on ITO-coated silicon wafers, at 700°C for 300 minutes.

[Fig. 8(a)] shows the isothermal grain growth curve of grain size vs. growing time at 700°C for all samples with the same initial grain sizes. It demonstrates that the grain growth behavior of isothermal hold follows a more gradual process than the one of heating up.

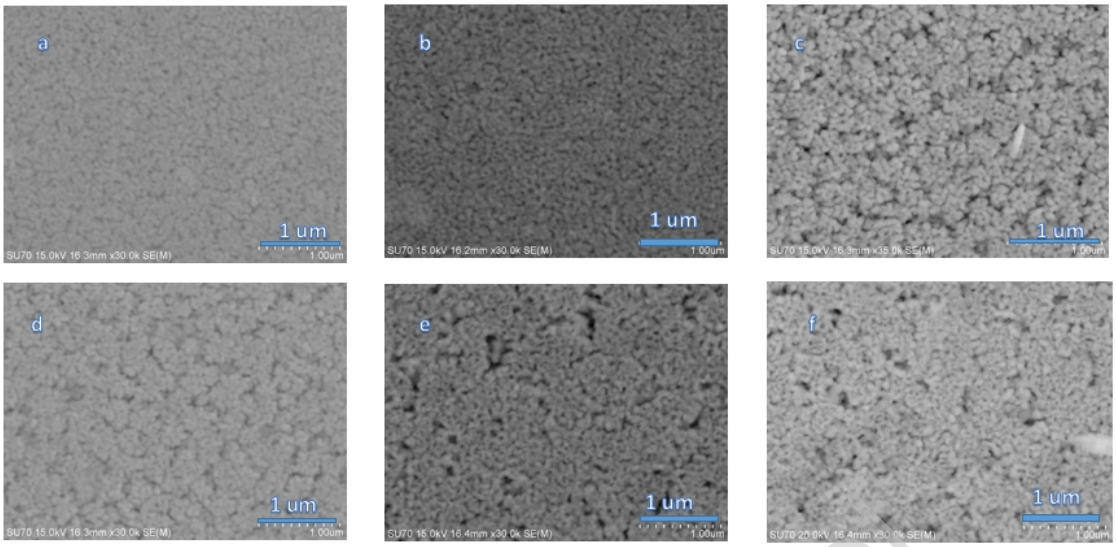

Fig. 8 (a). The SEM Micrograph of BaTiO3 film sintered at 700ºC for (a) 10 minutes; (b) 30 minutes; (c) 60 minutes; (d) 100 minutes; (e) 300 minutes; and (f) 600 minutes.

The TEM Micrograph of $BaTiO_3$ [Fig. 8(b)] shows that, with grains which are sintered at 700ºC for a different time, the arrangement of the inner grain atoms is almost the same but the directions of atoms are different.

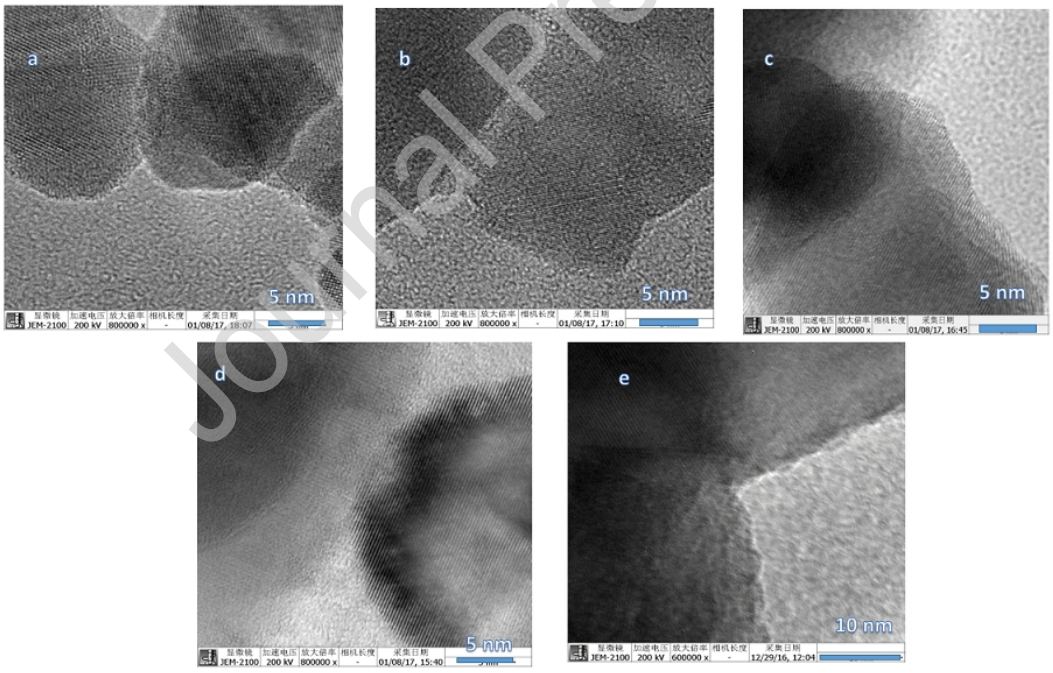

Fig. 8 (b). The TEM Micrograph of BaTiO3 grain sintered at 700ºC for (a) 1 minute; (b) 30 minutes; (c) 100 minutes; (d) 300 minutes; and (e) 600 minutes.

3.2.4. The sintering consolidation process and the influence of fractal nature

3.2.4.1 The kinetic exponent of grain growth for isothermal sintering

Generally, grain growth occurs in polycrystalline materials to decrease the free energy of a system by decreasing the total grain boundary energy. The grain growth behavior of polycrystalline materials was reported and integrated into the following equation where the rate of grain growth is inversely proportional to grain size:

$$D_G^{\,k} - D_{G_0}^{\,k} = c_0 \cdot t \tag{8}$$

Here, D_G is the average grain size at the time t; D_{G0} is the initial average grain size; k is the grain growth exponential reflecting grain growth behavior; and, c_0 is the temperature-dependent rate constant that could be expressed by the Arrhenius equation:

$$c_0 = A_r\, e^{-E/RT} \tag{9}$$

where A_r is pre-exponential factor; E is the activation energy; R is the universal gas constant; and T is temperature. In this case, a constant sintering temperature is assumed.

Since D_{G0} is generally much smaller than D_G i.e. ($D_G >> D_{G_0}$), D_G is reduced to

$$D_G = c_1 \cdot t^{1/k} \tag{10}$$

Since, $A_G = \left(D_G / 2\right)^2 \pi$, where A_G is normal grain size, from [Eq. (10)] it follows that

$$A_G = c_2 \cdot t^{2/k} \tag{11}$$

taking Log we get:

$$\text{Log } A_G = (2/k)\ \text{Log t} + C_3 \tag{12}$$

which, when plotted in a logarithmic scale, is a straight line with slope of 2/k. k is the kinetic exponent of grain growth, A_G is the average grain area, and C_3 is constant. Kinetic exponent k can be obtained from the slope of the linear regression line of Log A_G versus Log t.

As all of the grain areas can be collected during the sintering process, average grain areas in different grains can be calculated by image J or manually. Therefore, the average grain area versus growth time can be plotted in a logarithmic scale. The kinetic exponents of grain growth correspond inversely to the slope of the curve. They are approximately 0.0651 at the early stages of the sintering process and then increase to 0.2543 at later stages, as shown in [Fig. 8(c)]. It can be seen that the kinetic exponents of grain growth are actually a function of time. At an early stage of sintering, it has a lower kinetic energy than those at a later stage of process because, at the chosen temperature of 700**°**C, polymer materials have not been completely removed from the structure. Normal grain growth (primary recrystallization) is controlled.

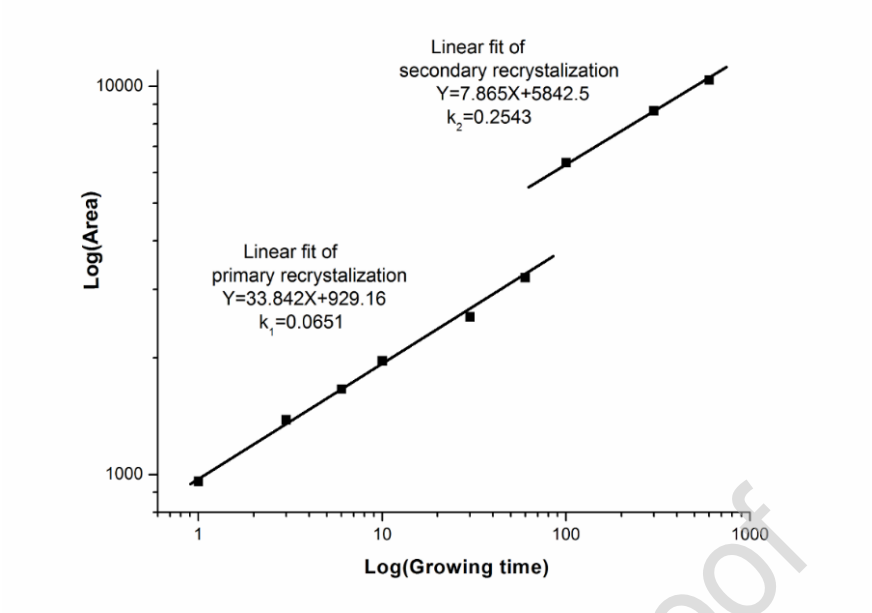

Fig. 8 (c). Grain area vs. growth times $BaTiO_3$ film at 700° C.

According to [Fig. 8(d)], the variation of fractal dimensions of the nanostructure $BaTiO_3$ sintered at different soaking times, can be distributed as follows: the largest fractal dimension reduction at the time of 10 min indicates a rearrangement of grains and the withdrawal of carbon from the structure. The fractal dimension will then increase until the carbon has been completely removed from the structure at around 100 min from the beginning of sintering. When the fractal dimension decreases, this means that the surfaces of grain boundaries will become smoother with growth time and self-similarity will decrease, which may be indicative of the onset of an abnormal grain growth.

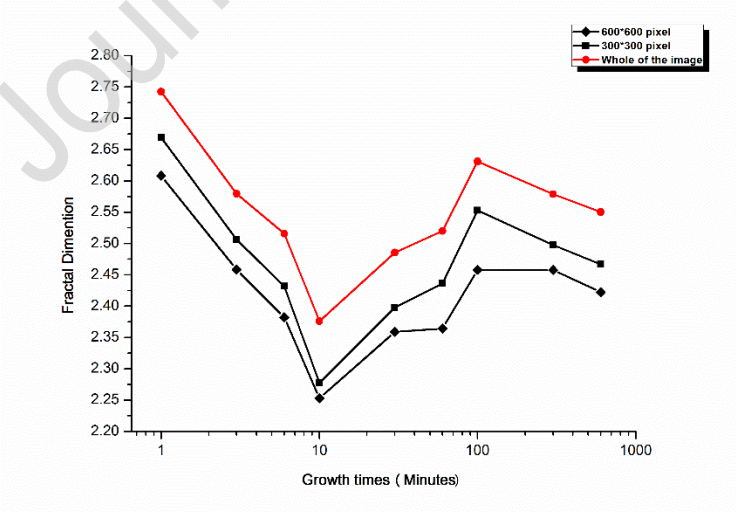

Fig. 8 (d). Variation of fractal dimension of nano structure BaTiO3 sintered at different soaking time.

3.2.4.2 The influence of fractal correction on sintering temperature

In case we don't have a constant sintering temperature, we can apply α-complex fractal correction on the sintering temperature T in the basic Arrhenius equation. In this case, the sintering time t is constant. Also, the grain growth exponential factor k, reflecting the kinetics of grain growth, is temperature T dependent.

It is an experimental fact that most rate constants of reactions vary with temperature in a common fashion: nearly always, Log k is linear with 1/T. Arrhenius was first to recognize the generality of this behavior and he proposed that rate constants be expressed in the form

$$k = A_r e^{-\frac{E_a}{RT}} \tag{13}$$

Ar: the pre-exponential factor (a constant for each reaction)
Ea: the activation energy for the reaction
R: gas constant 8.3144598 J · mol−1 · K−1
T: absolute temperature

Pre-exponential factor is considered the probability to surmount energy barrier of height E_a (the activation energy), by using thermal energy. While the exponential expresses the probability of surmounting the barrier, A_r must be related to the frequency of attempts on it; thus A_r is considered the frequency factor. By the collision theory, frequency factor is given by:

$$A_r = \left(\frac{\sigma_1 + \sigma_2}{2}\right)^2 \pi \sqrt{\frac{8k_B T}{\pi}\left(\frac{1}{m_1} + \frac{1}{m_2}\right)} \tag{14}$$

where

m_i : mass of particle i (i=1,2);
σ_i : diameter of particle i (i=1,2);
k_B : Boltzman's constant.

Regarding the reaction rate which is proportional to absolute temperature, our hypothesis is that particles with mass m_i and diameter σ_i Brownian motion (α_M) within the bulk sintering process, influence the rate of reaction.

Also, in the case of grains and pore surfaces (α_S, α_P), morphology influence, within this complex sintering reaction, is evident and very important.

Through physical-mathematical grain and pore micro surface analysis, we have established the presence of fractal nature in this morphology, which is confirmed by the fractal reconstruction of many microstructures [46, 47, 48].
Finally,

$$A_r = A_0 \sqrt{\alpha_f T} \tag{15}$$

$$\alpha_f = \Phi\left(\alpha_S, \alpha_P, \alpha_M\right) \tag{16}$$

We suppose that the involvement of these fractal corrections α_S , α_f , α_M in the overall fractal correction α_f is given by the weighted sum [49, 50, 51]:

$$\alpha_f = w_1\alpha_S + w_2\alpha_P + w_3\alpha_M, \quad w_1 + w_2 + w_3 = 1 \tag{17}$$

We take a normalized fractal dimension as the representation of a fractal nature. So, the individual fractal corrections will be:

$$\alpha_S = \dim \overline{X1}(u,v) = \dim \sum_{i=1}^{m}\sum_{j=1}^{n}\left(1 + R1\left(\varphi_i,\theta_j\right)\right)\begin{pmatrix}\sin\varphi\sin\theta\\ \cos\varphi\sin\theta\\ \cos\theta\end{pmatrix} B_i^{\Phi}(\varphi)B_j^{\Theta}(\theta) - 2, \quad 0 \le \alpha_S \le 1 \tag{18}$$

$$\alpha_P = \dim \overline{X2}(u,v) = \dim \sum_{i=1}^{m}\sum_{j=1}^{n}\left(1 + R2\left(\varphi_i,\theta_j\right)\right)\begin{pmatrix}\sin\varphi\sin\theta\\ \cos\varphi\sin\theta\\ \cos\theta\end{pmatrix} B_i^{\Phi}(\varphi)B_j^{\Theta}(\theta) - 2, \quad 0 \le \alpha_P \le 1 \tag{19}$$

$$\alpha_M = \dim \overline{X}(t) = \dim \sum_{i=0}^{n} X(t_i)B_i(t) - 1, \quad 0 \le \alpha_M \le 1 \tag{20}$$

The overall fractal correction is a problem of exceptional complexity so, at first, we assume the equal participation of each individual fractal correction:

$$\begin{aligned}\alpha_f &= \frac{1}{3}\alpha_S + \frac{1}{3}\alpha_P + \frac{1}{3}\alpha_M \\ &= \frac{1}{3}\left(\dim \sum_{i=1}^{m}\sum_{j=1}^{n}\left(1 + R1\left(\varphi_i,\theta_j\right)\right)\begin{pmatrix}\sin\varphi\sin\theta\\ \cos\varphi\sin\theta\\ \cos\theta\end{pmatrix} B_i^{\Phi}(\varphi)B_j^{\Theta}(\theta) - 2\right) \\ &+ \frac{1}{3}\left(\dim \sum_{i=1}^{m}\sum_{j=1}^{n}\left(1 + R2\left(\varphi_i,\theta_j\right)\right)\begin{pmatrix}\sin\varphi\sin\theta\\ \cos\varphi\sin\theta\\ \cos\theta\end{pmatrix} B_i^{\Phi}(\varphi)B_j^{\Theta}(\theta) - 2\right) \\ &+ \frac{1}{3}\left(\dim \sum_{i=0}^{n} X(t_i)B_i(t) - 1\right)\end{aligned} \tag{21}$$

Obviously $0 \le \alpha_f \le 1$.

The argument for this expectation is, in fact, that the geometrically irregular motion of an enormous number of particles causes extra energy to be unleashed onto the system. So, in this way, we have definitely analyzed all the aspects of sintering process, which, beside sintering time also include sintering temperature. All of this fractal corrections are based on previous experimental results and analysis. So, here is not just theoretical mathematical correction, these corrections are confirmed through the different experimental analysis so, here is just application of generalized confirmed results.

4. Conclusion

Barium-titanium oxide films were obtained successfully by spin coating of sol gel precursors. The results of TG and DTA indicate that decomposition of sol-gel occurs in different stages. The XRD analysis of $BaTiO_3$ films sintered at 700°C for 2 hours, shows that the main diffraction peaks become narrower and sharper than those sintered at lower temperatures. The grain growth behavior under isothermal hold conditions follows a more gradual process than that of a gradual heat-up.

The kinetic exponent of grain growth in the secondary recrystallization is larger than that of a primary recrystallization at 700°C.

The fractals of ceramic microstructure changed at different temperatures and soaking times. Therefore, the fractal dimensions can be taken as an influence parameter of grain growth for the process, including isothermal holding and can indicate pore removal during sintering process.
In this paper, the grains are not individually examined so the interpretation of changing properties and process is easier.

On the other hand, we have developed and applied new fractal methods and tools when the sintering temperature T is varying at the constant sintering time. This is one of the first papers in which physico-mathematical fractal analysis is fully applied. This new approach has opened a new frontier in this area, especially in the fractalization of the sintering process, as well as new perspectives for further breakthroughs in the field of sintering analysis.

Acknowledgements

The authors are extremely grateful for the assistance of Prof. Hiroyuki Sasaki in providing the FRACTAL ANALYSIS SYSTEM Software, version 3.4.7. The authors appreciate the efforts and support of Professor Xiong Zhaoxian, a knowledgeable and memorable person, and, finally, the authors thank Mr. Quint Feldman for helping us with editing this paper.

References

[1] Waugh, Mark D, Design solutions for DC bias in multifilm ceramic capacitors, Electronic Engineering Times (2010).

[2] Daining Fang JinXi Liu, Fracture mechanics of Piezoelectric and Ferroelectric solids, Tsinghua University Press/Springer, Beijing (2014).

[3] Tetsuro Tanka, Barium Titanate Ceramics and their Applications, Bull. Inst. Chem. Res. Kyoto Univ.32(2) (1954) 43–53.

[4] M.T. Buscaglia, M. Viviani, V. Buscaglia, L. Mitoseriu, A. Testino, P. Nanni, “High dielectric constant and frozen macroscopic polarization in dense nanocrystallineBaTiO3 ceramics”, Phys. Rev. B 73 (2006).

[5] H. Chazono and H. Kishi, Jap. J. Appl. Phys. 40 (9B) 5624 (2001).

[6] Jianjun Tian, Huiping Gao, Weibing Deng, Haiwu Zheng, Furui Tan, Weifeng Zhang, Optical properties of Fe-doped BaTiO3 films deposited on quartz substrates by sol-gel method, Journal of Alloys and Compounds 687 (2016).

[7] Zhu, Jinlong & Jin, Changqing & Cao, Wenwu & Wang, Xiaohui, Phase Transition and Dielectric Properties of Nanograin BaTiO3 Ceramic Under High Pressure, Applied Physics Letters. 92 (2008).

[8] Ghayour, Hamid & Abdellahi, Majid. (2016). A brief review of the effect of grain size variation on the electrical properties of BaTiO3-based ceramics. Powder Technology 292 (2016).

[9] Hoshina T. Size effect of barium titanate: Fine particles and ceramics [J]. Journal-Ceramic Society Japan, 2013, 121(1410):156-161.

[10] J. E. Kim, C. H. Song, and H. W. Park, Mater. Sci. Eng. A 449-451, 299 (2007).

[11] J. Das, K. Chandra, P.S. Misra, B. Sarma, Novel powder metallurgy technique for development of Fe–P-based soft magnetic materials, J. Magn. Magn. Mater. 320 (2008) 906–915.

[12] G.V. Samsonov, V.I. Yakovlev, Activated sintering of tungsten with nickel additions, Powder Metall. Met. Ceram. 6 (8) (1967) 606–611.

[13] Brinker, C. And Scherer, G., Sol Gel Science: The Physics And Chemistry Of Sol Gel Processing, Academic Press Inc. (1990).

[14] Wright JD, Sommerdijk NAJM. Sol–gel materials: chemistry andapplications, CRC Press(2000).

[15] K.N. Ramakrishnan, S. Venkadesan, K.P.N. Murthy, A fractal description of grain boundaries in a sintered powder metallurgical sample, Scr. Metall. Mater. 32 (1995) 685–688.

[16] G. Reisel, R.B. Heimann, Correlation between surface roughnesses of plasma sprayed chromium oxide coatings and powder grain size distribution: a fractal approach, Surf. Coat. Technol. 185 (2004) 215–221.

[17] Zuo R, Wang J. Fractal/multifractal modeling of geochemical data: A review [J]. Journal of Geochemical Exploration, 2016, 164:33-41.

[18] P. Embrechts and M. Maejima, An introduction to the theory of self-similar stochastic processes, International Journal of Modern Physics B, vol. 14, pp. 1399-1420, 2000.

[19] B. B. Mandelbrot, The fractal geometry of nature: Macmillan, 1983.

[20] A. L. Goldberger, D. R. Rigney, and B. J. West, "Science in pictures: Chaos and fractals in human physiology," Scientific American, vol. 262, pp. 42-49, 1990.

[21] A.J. Hickey, N.M. Concessio, Descriptors of irregular particle morphology and powder properties, Adv. Drug Deliv. Rev. 26 (1997) 29–40.

[22] T. Akiyama, T. Iguchi, K. Aoki, K. Nishimoto, A fractal analysis of solids mixing in two-dimensional vibrating particle beds, Powder Technol. 97 (1998) 63–71.

[23] C.Y. Poont, R.S. Sayles, T.A. Jones, Surface measurement and fractal characterization of naturally fractured rocks, J. Phys. D Appl. Phys. 25 (1992) 1269–1275.

[24] L.C.Y. Chan, N.W. Page, Particle fractal and load effects on internal friction in powders, Powder Technol. 90 (1997) 259–266.

[25] N. Bird, M. Cruz Díaz, A. Saa, A.M. Tatquis, Fractal and multifractal analysis of pore-scale images of soil, Journal of Hydrology 322 (2006) 211–219.

[26] A. Dathe, M. Thullner, The relationship between fractal properties of solid matrix and pore space in porous media, Geoderma 129 (3) (2005) 279–290.

[27] Li LM, Ji GL, Yang YP, et al. Practical Evolutions and Computer Simulation of Pores in $BaTiO_3$ Ceramics during Sintering Process [J]. Key Engineering Materials, 2008, 368-372:1585-1587.
[28] Xiong Z. X, Baba-Kishi K Z, Shin F G, et al. Microstructural characterization of ferroelectric Pb(Sc0.5Ta0.5)O3 ceramics[J]. Ferroelectrics, 1999, 229(1):153-158.

[29] H. E. Hurst, "Long-term storage capacity of reservoirs," Trans. Amer. Soc. Civil Eng., vol. 116,pp. 770-808, 1951.

[30] Hambly B M. Ch. 10. Fractals and the modelling of self-similarity [J]. Handbook of Statistics, 2003, 21(03): 371-406.

[31] Lee W L, Hsieh K S. A robust algorithm for the fractal dimension of images and its applications to the classification of natural images and ultrasonic liver images [J]. Signal Processing, 2010, 90(6):1894-1904.

[32] Tang HP, Wang JZ, Zhu JL, et al. Fractal dimension of pore-structure of porous metal materials made by stainless steel powder [J]. Powder Technology, 2012, 217(2):383-387.

[33] Liu Y, Wang C, Zhang Y, et al. Fractal process and particle size distribution in a TiH2, powder milling system [J]. Powder Technology, 2015, 284:272-278.

[34] Atzeni C, Pia G, Sanna U. Fractal modelling of medium–high porosity SiC ceramics [J]. Journal of the European Ceramic Society, 2008, 28(14): 2809-2814.

[35] Sánchez-López J C, Fernández A. TEM study of fractal scaling in nanoparticle agglomerates obtained by gas-phase condensation[J]. Acta Materialia, 2000, 48(14):3761-3771.

[36] Galindo-Hernández F, Portales B, Domínguez JM, et al. Porosity and fractal study of functionalized carbon nanofibers: Effects of the functionalization degree on hydrogen storage capacity [J]. Journal of Power Sources, 2014, 269(3):69- 80.

[39] iu Y, Lin J, Chen K. A Stable Algorithm of Box Fractal Dimension and Its Application in Pore Structure [J]. Rare Metal Materials & Engineering, 2015, 44(4): 800-804.

[40] Glass HJ, With G D. Fractal characterization of the compaction and sintering of ferrites [J]. Materials Characterization, 2001, 47(1): 27-37.

[41] Mitic VV, Paunovic V, Kocic L. Fractal approach to BaTiO3-ceramics micro-impedances [J]. Ceramics International, 2015, 41(5): 6656-6574.

[42] Mitic VV, Paunovic V, Purenovic J, et al. The contribution of fractal nature to BaTiO3-ceramics microstructure analysis [J]. Ceramics International, 2012, 38(2):1295-1301.

[43] Mitic VV, Paunovic V, Purenovic J, et al. Processing parameter influence on BaTiO3 ceramic fractal microstructure and dielectric characteristics [J]. Advances in Applied Ceramics, 2012, 111(5-6):360-366.

[44] Mitic VV, Paunovic V, Pavlovic V, et al. Sintering process influence on microstructure and intergranular impedance of rare-earth modified BaTiO3-ceramics [J]. Science of Sintering, 2011, 43(3):277-287.

[45] Sarkar N, Chaudhuri B B. An efficient differential box-counting approach to compute fractal dimension of image [J]. IEEE Trans.syst.man Cybern, 1994, 24(1): 115-120.

[46] Nayak SR, Mishra J, Jena P M. Fractal analysis of image sets using differential box counting techniques [J]. International Journal of Information Technology, 2018, 10(1): 39-47.

[47] Barnsley, M. (1993) Fractals Everywhere, Academic Press, (2nd Ed.), San Diego.

[48] Even U., Rademann K., Jortner J., Manor N. and Reisfeld R. (1984) Direct Electronic Energy Transfer on Fractals, Journal of Luminescence 31 & 32 634-638.

[49] Vojislav V. Mitić, Ljubiša M. Kocić, Steven Tidrow, Hans-Jörg Fecht, Structures, Fractals and Energy, Nanotechnology for Energy Sustainability, 2 Vol., 2017, (Baldev Raj, Marcel Van de Vorde, Yashwant Mahajan eds.),Wiley-VCH

[50] Vojislav V. Mitić, Vesna Paunović, Goran Lazović, Ljubiša Kocić & Branislav Vlahović, Clausius–Mossotti relation fractal modification, Ferroelectrics, 2018, 536:1, 60-76

[51] V.V. Mitic, Lj. Kocic, V. Paunovic, G. Lazović, M. Miljkovic, Fractal nature structure reconstruction method in designing microstructure properties, Materials Research Bulletin, 2018, 101:175-183

[52] Curecheriu, L., Balmus, S. B., Buscaglia, M. T., Buscaglia, V., Ianculescu, A., & Mitoseriu, L. (2012). Grain size-dependent properties of dense nanocrystalline barium titanate ceramics. Journal of the American Ceramic Society, 95(12), 3912-3921.

[53] Frey, M. H., & Payne, D. A. (1996). Grain-size effect on structure and phase transformations for barium titanate. Physical Review B, 54(5), 3158.

[54] Cai, Z., Wang, X., Hong, W., Luo, B., Zhao, Q., & Li, L. (2018). Grain-size–dependent dielectric properties in nanograin ferroelectrics. Journal of the American Ceramic Society, 101(12), 5487-5496.

[55] Yu, Boming, and Jianhua Li., Some fractal characters of porous media, Fractals 9.03 (2001): 365-372.

[56] Chi, Congcong, et al., Effect of Acetic Acid Pretreatment on Wood Pore Structure and Fractal Dimension, BioResources 12.2 (2017): 3905-3917.

Highlights

- *Analisy BaTiO3 nanograin growth with the sintering parameters influence on kinetics*
- *All of these sintering analysis we are enriching with fractal nature approach*
- *New approach enlight consolidation and morphology by fractal nature analysis*
- *The fractal dimension characterisation is included to complete analysis*
- *Here, we introduce the fractal nature correction influence on sintering temperature*